

Study of the process $e^+e^- \rightarrow \eta\gamma$ in the center-of-mass energy range 1.07–2.00 GeV

M. N. Achasov,^{1,2} V. M. Aulchenko,^{1,2} A. Yu. Barnyakov,¹ K. I. Beloborodov,^{1,2} A. V. Berdyugin,^{1,2,*}
 A. G. Bogdanchikov,¹ A. A. Botov,¹ T. V. Dimova,^{1,2} V. P. Druzhinin,^{1,2} V. B. Golubev,^{1,2}
 K. A. Grevtsov,^{1,2} L. V. Kardapoltsev,^{1,2} A. G. Kharlamov,^{1,2} D. P. Kovrizhin,¹ I. A. Koop,^{1,2}
 A. A. Korol,^{1,2} S. V. Koshuba,¹ A. P. Lysenko,¹ K. A. Martin,¹ A. E. Obrazovsky,¹ E. V. Pakhtusova,¹
 E. A. Perevedentsev,^{1,2} A. L. Romanov,¹ S. I. Serednyakov,^{1,2} Z. K. Silagadze,^{1,2} A. N. Skrinsky,¹
 I. K. Surin,¹ Yu. A. Tikhonov,^{1,2} A. V. Vasiljev,^{1,2} P. Yu. Shatunov,¹ Yu. M. Shatunov,^{1,2} and D. A. Shtol¹

¹*Budker Institute of Nuclear Physics, SB RAS, Novosibirsk, 630090, Russia*

²*Novosibirsk State University, Novosibirsk, 630090, Russia*

The $e^+e^- \rightarrow \eta\gamma$ cross section has been measured in the center-of-mass energy range 1.07–2.00 GeV using the decay mode $\eta \rightarrow 3\pi^0$, $\pi^0 \rightarrow \gamma\gamma$. The analysis is based on 36 pb^{-1} of integrated luminosity collected with the SND detector at the VEPP-2000 e^+e^- collider. The measured cross section of about 35 pb at 1.5 GeV is explained by decays of the $\rho(1450)$ and $\phi(1680)$ resonances.

PACS numbers: 13.66.Bc, 13.20.Gd, 13.40.Hq, 14.40.Be

I. INTRODUCTION

Radiative decays are a powerful tool for studying the internal structure of hadrons. For light vector mesons, these decays have been investigated in several experiments over the past 40 years. The probabilities of the ρ , ω and ϕ decays to $\eta\gamma$ are currently measured with accuracies of 7%, 9% and 2%, respectively. For the ρ and ω mesons, the errors are still dominated by statistics. The most accurate measurements of the light vector meson decays to $\eta\gamma$ were performed in the SND [1] and CMD-2 [2] experiments at the VEPP-2M e^+e^- collider. These measurements will be continued with more statistics at the VEPP-2000 collider [3].

In e^+e^- experiments a directly measured quantity is the cross section for $e^+e^- \rightarrow \eta\gamma$. The cross section is measured in a wide range of the center-of-mass (c.m.) energies, for example, from 0.6 to 1.4 GeV at VEPP-2M [1, 2]. The decay probabilities are then derived from the fit to the cross-section data with a sum of vector-resonance contributions. When analyzing the VEPP-2M data, it was found that the model errors on the probabilities of the ρ , ω , $\phi \rightarrow \eta\gamma$ decays associated with uncertainties of contributions of excited vector states, can reach several percents. To diminish this uncertainty the measurement of the cross section for $e^+e^- \rightarrow \eta\gamma$ is required at energies at least up to 2 GeV.

Measurement in the 1–2 GeV energy range is also interesting in itself. From the cross section data we can derive the probabilities of radiative decays of excited vector mesons, such as the $\rho(1450)$ and $\phi(1680)$. In this energy region, besides the normal $q\bar{q}$ vector states, production of exotic hybrid (quark-antiquark-gluon) mesons is expected. Since hybrid states can be mixed with the conventional quark-antiquark states, their identification is a difficult experimental problem requiring a detailed analysis of all possible decay modes. Radiative decays, the probabilities of which are expected to be relatively well predicted in the framework of the quark model, may play the key role in the identification of the hybrid vector states.

In this article we present a measurement of the $e^+e^- \rightarrow \eta\gamma$ cross section in the energy range 1.07–2.00 GeV in an experiment with the SND detector at the VEPP-2000 e^+e^- collider [3].

II. DETECTOR AND EXPERIMENT

We analyze data with an integrated luminosity of about 40 pb^{-1} accumulated in 2010–2012. During the experiments, the energy range 1.05–2.00 GeV was scanned several times with a step of 20–25 MeV. In this analysis, because of the low statistics, we measure the cross section values averaged over ten energy intervals listed in Table I.

A detailed description of the SND detector is given in Ref. [4]. This is a nonmagnetic detector, the main part of which is a three-layer spherical electromagnetic calorimeter based on NaI(Tl) crystals. A solid angle covered by the calorimeter is 90% of 4π . Its energy resolution for photons is $\sigma_E/E = 4.2\%/\sqrt[4]{E(\text{GeV})}$, and the angular resolution

*e-mail:berdugin@inp.nsk.su

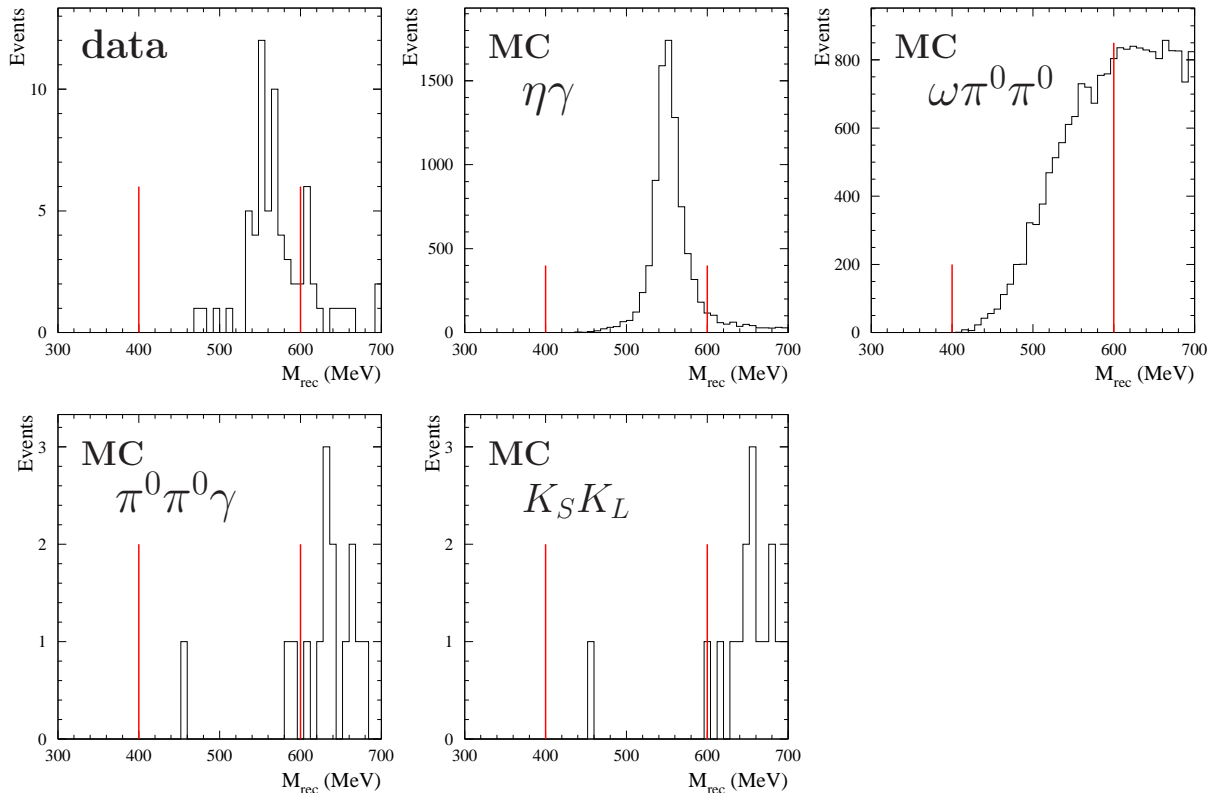


FIG. 1: The M_{rec} distributions for data and simulation of the signal and background processes. The vertical lines indicate the selection boundaries.

about 1.5° . Directions of charged particles are measured in the tracking system consisting of a nine-layer drift chamber and a proportional chamber with readout from cathode strips. The drift chamber provides solid angle coverage of 94% of 4π .

The process $e^+e^- \rightarrow \eta\gamma$ is studied in the decay mode $\eta \rightarrow 3\pi^0 \rightarrow 6\gamma$. Since the final state under study does not contain charged particles, for normalization we choose the process without charged particles, $e^+e^- \rightarrow \gamma\gamma$. As a result of such normalization, systematic uncertainties associated with the event selection in the hardware first-level trigger are canceled, as well as uncertainties arising from superimposing beam-generated spurious tracks onto the events being studied. The uncertainty on the luminosity measurement with the process $e^+e^- \rightarrow \gamma\gamma$ is estimated to be 2.2% [5].

III. EVENT SELECTION

The main decay modes of the η meson are 2γ (39%), $3\pi^0$ (33%) and $\pi^+\pi^-\pi^0$ (23%). Background from the processes $e^+e^- \rightarrow 3\gamma$ and $e^+e^- \rightarrow \pi^+\pi^-\pi^0$ significantly exceeds the signal in the energy range 1.07–2.00 GeV and does not allow to use the decay modes $\eta \rightarrow 2\gamma$ and $\eta \rightarrow \pi^+\pi^-\pi^0$. Thus, in this paper, the process $e^+e^- \rightarrow \eta\gamma$ is studied in the decay channel $\eta \rightarrow 3\pi^0$, $\pi^0 \rightarrow 2\gamma$ having seven photons in the final state.

The main sources of background in this analysis are the processes $e^+e^- \rightarrow K_S K_L(\gamma)$ with $K_S \rightarrow 3\pi^0$, $e^+e^- \rightarrow \pi^0\pi^0\gamma$ and $e^+e^- \rightarrow \omega\pi^0\pi^0$, $\omega \rightarrow \pi^0\gamma$, of which only the latter has seven photons in the final state. In the process $e^+e^- \rightarrow K_S K_L$, additional spurious photons originate from K_L nuclear interactions in the calorimeter. In the process $e^+e^- \rightarrow \omega\pi^0 \rightarrow \pi^0\pi^0\gamma$, extra photons can be reconstructed due to splitting of the electromagnetic showers, photon emission by the initial particles at a large angle, and superimposing beam-generated background.

Event selection is carried out in two stages. At the first stage we select events containing at least seven photons and no charged particles. The events must satisfy the following conditions on the total energy deposition in the calorimeter (E_{tot}) and the total momentum of photons (P_{tot}):

$$0.7 < E_{tot}/2E_{beam} < 1.2, \quad cP_{tot}/2E_{beam} < 0.3, \quad E_{tot}/2E_{beam} - cP_{tot}/2E_{beam} > 0.7. \quad (1)$$

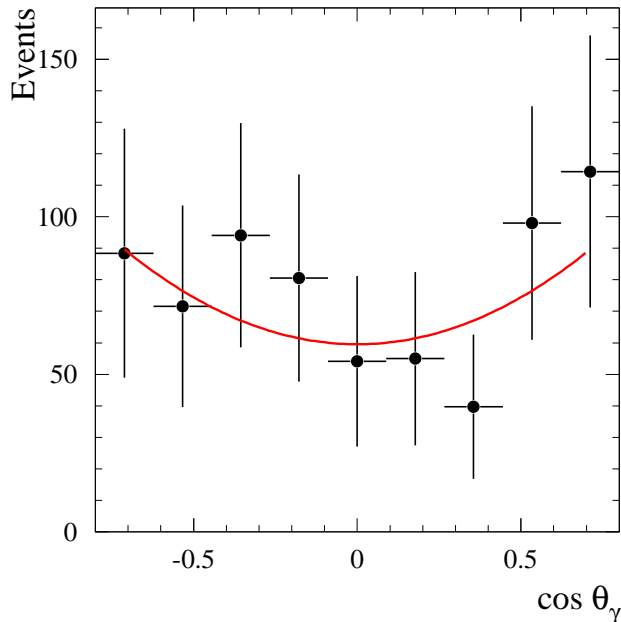


FIG. 2: The efficiency-corrected distribution of the cosine of the recoil-photon polar angle for selected data events. The curve is a fit to data with $A(1 + \cos^2 \theta_\gamma)$.

At the second stage, kinematic fits are performed for selected events with requirements of energy-momentum conservation and π^0 mass constraints. As a result of the kinematic fit, we obtain corrected photon energies and χ^2 for the kinematic hypothesis used. Two hypotheses are tested:

- $e^+e^- \rightarrow 3\pi^0\gamma$ ($\chi_{3\pi^0\gamma}^2$),
- $e^+e^- \rightarrow \pi^0\pi^0\gamma$ ($\chi_{\pi^0\pi^0\gamma}^2$).

Under the $e^+e^- \rightarrow 3\pi^0\gamma$ hypothesis, it is assumed that the recoil photon is the most energetic in an event, and π^0 's are constructed from the remaining six photons. When photons additional within the tested hypothesis are present in the event, we check all possible five(seven)-photon combinations and use the one with the minimal value of $\chi_{\pi^0\pi^0\gamma}^2$ ($\chi_{3\pi^0\gamma}^2$). Further selection uses the following conditions:

$$\chi_{3\pi^0\gamma}^2 < 50, \chi_{\pi^0\pi^0\gamma}^2 > 20. \quad (2)$$

Under the $e^+e^- \rightarrow 3\pi^0\gamma$ kinematic hypothesis, the mass recoiling against the photon M_{rec} is calculated. The M_{rec} distributions for data as well as for simulation of the process under study and the background processes are shown in Fig. 1. It is seen that the signal process $e^+e^- \rightarrow \eta\gamma$ dominates in the data distribution. For the final event selection, the condition $400 < M_{rec} < 600$ MeV/ c^2 is used.

Figure 2 shows the $\cos\theta_\gamma$ distribution, where θ_γ is the recoil-photon polar angle, for selected data events with $\cos\theta_\gamma < 0.8$. The distribution is corrected to take into account the angular dependence of the detection efficiency. It is seen that the data are well described by the distribution $1 + \cos^2\theta_\gamma$ expected for $e^+e^- \rightarrow \eta\gamma$.

With the criteria described above, 60 events are selected. Their distribution over the energy intervals together with the expected background distribution is given in Table I. The background is estimated from MC simulation using the measured $\phi \rightarrow K_S K_L$ decay probability [6] and cross sections for the processes $e^+e^- \rightarrow K_S K_L$ [7], $e^+e^- \rightarrow \omega\pi^0 \rightarrow \pi^0\pi^0\gamma$ [5] and $e^+e^- \rightarrow \omega\pi^+\pi^-$ [8]. For the process $e^+e^- \rightarrow \omega\pi^0\pi^0$, we use the isotopic relation $\sigma(\omega\pi^+\pi^-) = 2\sigma(\omega\pi^0\pi^0)$ when calculating the background contribution. Our MC simulation takes into account radiative corrections [9]. This is particularly important for the background from the process $e^+e^- \rightarrow K_S K_L(\gamma)$, which is dominated by radiative return to the ϕ meson through the reaction $e^+e^- \rightarrow \phi\gamma$. The estimated number of background events is equal to 2.3 (0.4 from $K_S K_L(\gamma)$, 0.5 from $\pi^0\pi^0\gamma$ and 1.4 from $\omega\pi^0\pi^0$). The process $e^+e^- \rightarrow K_S K_L(\gamma)$ contributes only to the first interval. We conservatively estimate the systematic uncertainty in the background calculation to be 100% of the background calculated.

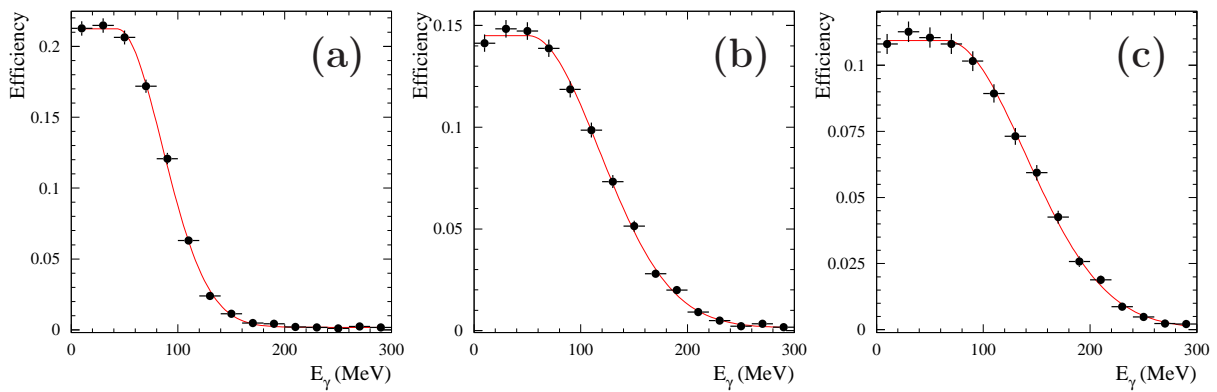


FIG. 3: The detection efficiency for $e^+e^- \rightarrow \eta\gamma$ events as a function of the energy of the additional photon emitted by initial particles for (a) $2E_{beam} = 1.1$ GeV, (b) $2E_{beam} = 1.6$ GeV, and (c) $2E_{beam} = 1.96$ GeV. The points with error bars are obtained using the MC simulation, the curve is the result of the $\epsilon(E_r)$ approximation by a smooth function.

IV. DETECTION EFFICIENCY

The detection efficiency for the process under study is determined using MC simulation, which takes into account the initial-state radiative corrections [9], in particular, emission of additional photons. The angular distribution of these photons is modeled according to Ref. [10].

The detection efficiency is determined as a function of two parameters: the c.m. energy and the energy of the additional photon E_r . Figure 3 shows the dependence of the detection efficiency on E_r for three different values of the c.m. energy. The values of the detection efficiency at $E_r = 0$, averaged over the corresponding energy intervals, are listed in the Table I.

V. FITTING THE VISIBLE CROSS SECTION AND EXTRACTION OF THE BORN CROSS SECTION

The visible cross section for $e^+e^- \rightarrow \eta\gamma$ directly obtained from the experimental data ($\sigma_{vis} = (N - N_{bkg})/IL$) is related to the Born cross section ($\sigma(E)$) by the expression:

$$\sigma_{vis}(E) = \int_0^{x_{max}} \epsilon_r(E, \frac{xE}{2}) F(x, E) \sigma(\sqrt{1-x}E) dx, \quad (3)$$

where $F(x, E)$ is a function [9] describing the distribution of the energy fraction, $x = 2E_r/E$, carried out by photons emitted from the initial state. Equation (3) can be rewritten in the traditional form:

$$\sigma_{vis}(E) = \epsilon(E) \sigma(E) (1 + \delta(E)), \quad (4)$$

where the detection efficiency $\epsilon(E)$ and the radiative correction $\delta(E)$ are defined as follows:

$$\epsilon(E) \equiv \epsilon_r(E, 0), \quad (5)$$

$$\delta(E) = \frac{\int_0^{\frac{2E_{r,max}}{E}} \epsilon_r(E, \frac{xE}{2}) F(x, E) \sigma(\sqrt{1-x}E) dx}{\epsilon_r(E, 0) \cdot \sigma(E)} - 1. \quad (6)$$

The Born cross section is determined as follows. The energy dependence of the measured visible cross section is fit with Eq. (3), in which the Born cross section is parametrized by a theoretical model that describes data reasonably well. The fitted model parameters are used to calculate the radiative correction according to Eq. (6). The experimental values of the Born cross section are then obtained using Eq. (4).

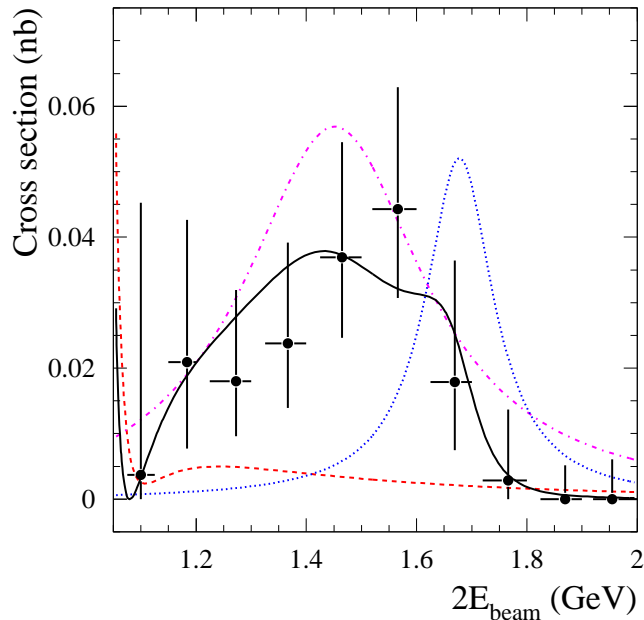


FIG. 4: The $e^+e^- \rightarrow \eta\gamma$ cross section measured in this work. The solid curve shows the result of the fit with the contributions of the ρ , ω , ϕ , ρ' and ϕ' resonances. The calculated cross section for $e^+e^- \rightarrow \rho, \omega, \phi \rightarrow \eta\gamma$ is shown separately (dashed curve) as well as the cross sections for $e^+e^- \rightarrow \rho' \rightarrow \eta\gamma$ (dot-dashed curve) and $e^+e^- \rightarrow \phi' \rightarrow \eta\gamma$ (dotted curve). Two latter curves are calculated using parameters obtained in the fit.

The energy dependence of the Born cross section for $e^+e^- \rightarrow \eta\gamma$ is parametrized according to the vector meson dominance (VMD) model:

$$\sigma_{\eta\gamma}(E) = \frac{k_\gamma(E)^3}{E^3} \left| \sum_{V=\rho, \omega, \phi, \dots} A_V(E) \right|^2, \quad A_V(E) = \frac{m_V \Gamma_V(m_V) e^{i\varphi_V}}{D_V(E)} \sqrt{\frac{m_V^3}{k_\gamma(m_V)^3} \sigma_{V\eta\gamma}}, \quad (7)$$

$$D_V(E) = m_V^2 - E^2 - iE\Gamma_V(E), \quad k_\gamma(E) = \frac{E}{2} \left(1 - \frac{m_\eta^2}{E^2} \right), \quad (8)$$

where $E = 2E_{beam}$, m_V is the mass of the vector resonance V , $\Gamma_V(E)$ is its energy-dependent total width, $\sigma_{V\eta\gamma} = (12\pi/m_V^2)B(V \rightarrow e^+e^-)B(V \rightarrow \eta\gamma)$ is the cross section for the process $e^+e^- \rightarrow V \rightarrow \eta\gamma$ at $E = m_V$, $B(V \rightarrow e^+e^-)$ and $B(V \rightarrow \eta\gamma)$ are the probabilities of the corresponding decays, φ_V is the resonance phase ($\varphi_\rho \equiv 0$). Besides ρ , ω and ϕ resonances, the sum includes all their excited states.

In the fit, parameters of the ρ , ω and ϕ resonances are fixed at the nominal values from the PDG tables [6]. The phases of the ρ , ω and ϕ contributions are chosen according to the quark model predictions: $\varphi_\omega = \varphi_\rho$, $\varphi_\phi = \varphi_\rho + 180^\circ$. At energy above 1 GeV the excited vector states $\omega(1420)$, $\rho(1450)$, $\omega(1650)$, $\phi(1680)$ and $\rho(1700)$ contribute to the $e^+e^- \rightarrow \eta\gamma$ cross section. Separation of these resonances in our fit is impossible. However, we can simplify the problem using the fact that the resonances are divided into two groups with similar masses, namely ($\omega(1420)$, $\rho(1450)$) and ($\omega(1650)$, $\phi(1680)$, $\rho(1700)$). With low statistics available we can use a fit model with two effective resonances ρ' and ϕ' with masses and widths equal to the PDG values for $\rho(1450)$ and $\phi(1680)$ [6]. Such a choice of resonances is consistent with predictions of the quark model [12], in which the decay widths of $\rho(1450) \rightarrow \eta\gamma$ and $\phi(1680) \rightarrow \eta\gamma$ are at least an order of magnitude larger than the corresponding widths for the three remaining excited states. The total widths of the ρ' and ϕ' in the formula (8) are assumed to be independent of energy.

The cross sections $\sigma_{\rho'\eta\gamma}$ and $\sigma_{\phi'\eta\gamma}$ are free fit parameters. For the phases $\varphi_{\rho'}$ and $\varphi_{\phi'}$ their canonical values [11] $\varphi_\rho + 180^\circ$ and $\varphi_\phi + 180^\circ$ are taken. The fit result is shown in Fig. 4 together with the values of the Born cross section calculated using Eq. (4). The numerical values of the Born cross section and radiative correction are listed in Table I. It should be noted that almost all data events in the first energy interval arise from the radiative return

TABLE I: The energy interval, integrated luminosity (IL), number of selected events (N), estimated number of background events (N_{bkg}), detection efficiency (ϵ_0), radiative correction ($\delta + 1$), $e^+e^- \rightarrow \eta\gamma$ Born cross section (σ). The first error in the cross section is statistical, the second systematic. For the last two energy intervals, the upper limits at the 90% confidence level are listed for the cross section.

$2E_{beam}$ (MeV)	IL (nb $^{-1}$)	N	N_{bkg}	ϵ_0 (%)	$\delta + 1$	σ (pb)
1075–1125	1962	25	0.4	7.43	45.8	$4_{-4}^{+41} \pm 20$
1150–1200	2093	4	0.1	6.94	1.28	$21_{-13}^{+22} \pm 2$
1225–1300	3250	4	0.2	6.99	0.93	$18_{-8}^{+14} \pm 2$
1325–1400	3367	5	0.2	6.52	0.92	$24_{-10}^{+15} \pm 2$
1425–1500	3600	8	0.3	6.23	0.93	$37_{-12}^{+18} \pm 2$
1520–1600	4351	10	0.5	5.26	0.94	$44_{-14}^{+19} \pm 2$
1625–1700	3016	3	0.3	5.21	0.96	$18_{-10}^{+19} \pm 2$
1720–1800	4675	1	0.2	4.53	1.34	$3_{-3}^{+11} \pm 1$
1825–1900	5134	0	0.1	4.34	1.64	< 6
1920–2000	4917	0	0.0	3.84	1.76	< 7

process $e^+e^- \rightarrow \phi\gamma$ and are actually background events.

The fitted values of the cross sections at the resonance peaks are following:

$$\begin{aligned}\sigma_{\rho' \rightarrow \eta\gamma} &= 57 \pm 10 \pm 7 \text{ pb}, \\ \sigma_{\phi' \rightarrow \eta\gamma} &= 52 \pm 17 \pm 15 \text{ pb}.\end{aligned}\tag{9}$$

The first error is statistical, the second systematic. The systematic errors were determined by varying the masses and widths of the excited resonances within the uncertainties of these parameters for $\rho(1450)$ and $\phi(1680)$. Figure 4 shows the cross sections of the processes $e^+e^- \rightarrow \rho' \rightarrow \eta\gamma$ and $e^+e^- \rightarrow \phi' \rightarrow \eta\gamma$, which correspond to the measured $\sigma_{\rho' \rightarrow \eta\gamma}$ and $\sigma_{\phi' \rightarrow \eta\gamma}$, and tails from the decays of ρ , ω and ϕ mesons, i.e. the $e^+e^- \rightarrow \rho, \omega, \phi \rightarrow \eta\gamma$ cross section. The fit results make it clear that the measured cross section cannot be successfully described without the contributions of excited vector mesons.

VI. SYSTEMATIC UNCERTAINTY OF THE MEASUREMENT

The systematic uncertainty on the measured cross section includes uncertainties in the detection efficiency determination, in the luminosity measurement, in the background estimation, and the model error in the radiative correction calculation.

To estimate the systematic uncertainty on the detection efficiency, we vary the selection criteria, in particular the condition on $\chi_{3\pi^0\gamma}^2$, within wide ranges and study the stability of the cross section results. We also perform the analysis with the requirement of detection of exactly seven photons in an event. At the existing level of statistical accuracy (60 detected events under the standard selection), no change of the cross section results is observed. To obtain numerical estimation of the uncertainty on the detection efficiency, we use the results of Ref. [5], where differences in the detector response between data and simulation were studied for the five-photon final state. Using much larger statistics, a correction to the detection efficiency determined from MC simulation was found to be $(-1.8 \pm 1.2)\%$. For current analysis, a sum of this correction and its error (3%) is taken as estimate of the uncertainty on the detection efficiency.

The luminosity is measured by using events of the two-photon annihilation with an accuracy of 2.2%. The systematic error in the number of selected signal events due to background subtraction is estimated to be equal to the number of background events.

To estimate the model error in the calculation of the radiative correction, we vary within the errors the masses and widths of the ρ' and ϕ' resonances. The largest effect comes, however, from variation of the phase of the ρ' amplitude which leads to a decrease of the dip in the cross section near 1.07 GeV. The change in the cross section due to variation resonance parameters and phases reaches 20 pb in the first energy interval and does not exceed 2 pb in the other. These values are taken as estimates of the model error. The numerical values of the total systematic uncertainties are listed in Table I.

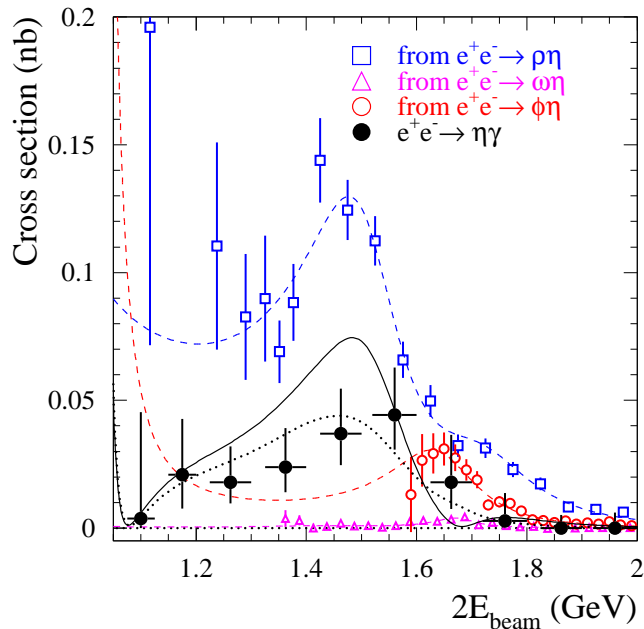


FIG. 5: The $e^+e^- \rightarrow \eta\gamma$ cross section measured in this work (\bullet) in comparison with the cross sections calculated using VMD from data on the processes $e^+e^- \rightarrow \rho\eta$ (\square), $e^+e^- \rightarrow \omega\eta$ (\triangle) and $e^+e^- \rightarrow \phi\eta$ (\circ). The dashed curves are results of the approximation of these cross sections by Eq. (7). The solid curve is the total cross section taking into account the interference of the isovector and isoscalar amplitudes. The dotted curve is the total cross section calculated using modified excited-state amplitudes (see the text).

VII. COMPARISON WITH THE DATA ON THE CROSS SECTIONS OF $e^+e^- \rightarrow V\eta$, $V = \rho, \omega, \phi$

Contributions to the $e^+e^- \rightarrow \eta\gamma$ cross section of the isovector and isoscalar $n\bar{n}$ ($n = u, d$) and $s\bar{s}$ states can be estimated from the cross sections for $e^+e^- \rightarrow \rho\eta$, $e^+e^- \rightarrow \omega\eta$ and $e^+e^- \rightarrow \phi\eta$, respectively, within the framework of the VMD model as follows:

$$\sigma_{\eta\gamma}(E) = \frac{4\pi\alpha}{f_V^2} \sigma_{V\eta} \frac{k_\gamma^3}{k_V^3}, \quad (10)$$

where f_V is the vector-meson-photon coupling constant, which is calculated from the vector meson electronic width: $f_V^2 = 4\pi m_V \alpha^2 / (3\Gamma(V \rightarrow e^+e^-))$. The vector meson momentum k_V for relatively narrow ω and ϕ resonances can be calculated as

$$k_V = \frac{1}{2E} \sqrt{((E + m_\eta)^2 - m_V^2) \cdot ((E - m_\eta)^2 - m_V^2)}. \quad (11)$$

For the ρ -meson one should use the exact formula that takes into account the finite width of the resonance [13].

Accuracy of Eq. (10) can be estimated from experimentally well-studied similar processes, for example, by comparing the measured decay width $\omega \rightarrow \pi^0\gamma$ with its VMD estimate from the decay $\omega \rightarrow \rho\pi \rightarrow \pi^+\pi^-\pi^0$ (see, for example, [17]). The estimate turns out to be 1.5 times larger than the actual width. One can therefore conclude that the typical accuracy of Eq. (10) is about 50%.

The calculated contributions to the $e^+e^- \rightarrow \eta\gamma$ cross section are shown in Fig. 5 in comparison with the cross section measured in this work. For the $e^+e^- \rightarrow \rho\eta$ cross section, experimental data from [8, 14] were used, while for the $e^+e^- \rightarrow \omega\eta$ and $e^+e^- \rightarrow \phi\eta$ cross sections data from Refs. [15, 16], respectively. It is seen that the contribution from the ω -like excited states is small. The VMD calculation confirms the predictions of the potential quark model [12] that the dominant contribution comes from the isovector and $s\bar{s}$ excited resonances. The calculated isovector cross section, even considering its 50% uncertainty, is significantly higher than the measured $e^+e^- \rightarrow \eta\gamma$ cross section. The difference can be reduced by a destructive interference of the isovector and $s\bar{s}$ amplitudes.

In order to calculate the interference effects, the cross sections derived by using Eq. (10) are fit with Eq. (7). For the isovector cross section, contributions from the $\rho(770)$, $\rho(1450)$ and $\rho(1700)$ only are considered. The isoscalar $s\bar{s}$ ($n\bar{n}$) cross section is described by a sum of the contributions of the $\phi(\omega)$ -like states.

Parameters (the mass, width and the peak cross section) for the $\rho(770)$, $\omega(782)$ and $\phi(1020)$ states are fixed at their PDG values [6]. Parameters of the excited resonances $\rho(1450)$, $\omega(1650)$ and $\phi(1680)$, which give the dominant contribution to the corresponding cross sections, are free fit parameters. The phase difference between the ground state and the first excitation is chosen to be 180° . Parameters of the $\rho(1700)$ and $\omega(1420)$ resonances are fixed at their PDG values [6]. For the phases of the $\omega(1650)$ and $\rho(1700)$ two options 0° and 180° were checked. In the case of the $\rho(1700)$, the best fit is obtained when the phase $\varphi_{\rho(1700)} = \varphi_\rho + 180^\circ$, while for the $\omega(1650)$ at the phase $\varphi_{\omega(1650)} = \varphi_\omega$. Note that because of the relative smallness of the $\rho(1700)$ and $\omega(1650)$ contributions, choice of these phases has little influence on the size and shape of the total cross section. The masses and widths of the $\rho(1450)$, $\omega(1650)$ and $\phi(1680)$ found in the fit are consistent with the PDG values [6]. The fit results are shown in Fig. 5 by the dashed curves.

The isovector and isoscalar $n\bar{n}$ and $s\bar{s}$ amplitudes obtained from the fit are combined with phases $\varphi_\omega = \varphi_\rho$ and $\varphi_\phi = \varphi_\rho + 180^\circ$. The resulting total cross section shown in Fig. 5 by the solid curve is in rather good agreement (considering the 50% uncertainty of the VMD calculation) with the measured cross section. A relatively small modification of the isovector and $s\bar{s}$ amplitudes (the $\rho(1450)$ and $\rho(1700)$ amplitudes are reduced by 15%, and the $\phi(1680)$ amplitude is increased by 25%) significantly improves this agreement. The cross section obtained after this modification is shown in Fig. 5 by the dotted curve.

Thus, our analysis in this section confirms that the dominant contribution to the cross section of $e^+e^- \rightarrow \eta\gamma$ in the energy range 1.1–2.0 GeV comes from the radiative decays of the two excited vector resonances $\rho(1450)$ and $\phi(1680)$.

VIII. CONCLUSION

The cross section for the process $e^+e^- \rightarrow \eta\gamma$ has been measured in the center-of-mass energy range from 1.07 to 2.00 GeV with the SND detector at the VEPP-2000 e^+e^- collider. Above 1.4 GeV, the cross section for this process has been measured for the first time. About 30 $e^+e^- \rightarrow \eta\gamma$ events detected at c.m. energy above 1.15 GeV cannot be explained within the VMD model with the $\rho(770)$, $\omega(782)$ and $\phi(1020)$ mesons only. We interpret these events as an observation of radiative decays of excited vector states into $\eta\gamma$.

From the combined analysis of the $e^+e^- \rightarrow \eta\gamma$ data obtained in this work and the data on the cross sections for $e^+e^- \rightarrow \rho\eta$, $e^+e^- \rightarrow \omega\eta$ and $e^+e^- \rightarrow \phi\eta$ we make the conclusion that the main contribution to the $e^+e^- \rightarrow \eta\gamma$ cross section above 1.1 GeV comes from the decays of the two excited meson states $\rho(1450)$ and $\phi(1680)$. For the processes $e^+e^- \rightarrow \rho(1450) \rightarrow \eta\gamma$ and $e^+e^- \rightarrow \phi(1680) \rightarrow \eta\gamma$, the following cross section values at the resonance peaks have been obtained:

$$\begin{aligned}\sigma_{\rho(1450) \rightarrow \eta\gamma} &= 57 \pm 10 \pm 7 \text{ pb}, \\ \sigma_{\phi(1680) \rightarrow \eta\gamma} &= 52 \pm 17 \pm 15 \text{ pb}.\end{aligned}\tag{12}$$

These cross sections can be compared with the predictions of the quark model. In Ref. [12] the following values for the partial decay widths were obtained: $\Gamma_{\rho(1450) \rightarrow \eta\gamma} \approx \Gamma_{\phi(1680) \rightarrow \eta\gamma} \approx 100$ keV. Using PDG values of the widths of the resonances and rough estimates of the total production cross sections of the $\rho(1450)$ (60 nb from the sum of the cross sections of $e^+e^- \rightarrow \pi^+\pi^-\pi^0\pi^0$ and $e^+e^- \rightarrow \pi^+\pi^-\pi^+\pi^-$ [18]), and $\phi(1680)$ (13 nb from the sum of the cross sections $e^+e^- \rightarrow K\bar{K}^*$ and $e^+e^- \rightarrow \phi\eta$ [16]) resonances in e^+e^- annihilation, we can estimate the cross sections $\sigma_{\rho(1450) \rightarrow \eta\gamma} \approx 15$ pb and $\sigma_{\phi(1680) \rightarrow \eta\gamma} \approx 10$ pb. It is seen that the decay widths of $\rho(1450) \rightarrow \eta\gamma$ and $\phi(1680) \rightarrow \eta\gamma$ obtained in Ref. [12] are too small to explain the observed $e^+e^- \rightarrow \eta\gamma$ cross section.

We thank S. I. Eidelman for useful discussions. This work is supported by the Ministry of Education and Science of the Russian Federation, the Russian Federation Presidential Grant for Scientific Schools NSh-5320.2012.2, RFBR (grants 12-02-01250, 12-02-00065, 13-02-00375, 13-02-00418), Grant 14.740.11.1167 from the Federal Program ‘‘Scientific and Pedagogical Personnel of Innovational Russia’’.

-
- [1] M. N. Achasov *et al.* (SND Collaboration), Phys. Rev. D **74**, 014016 (2006); **76**, 077101 (2007).
 - [2] R. R. Akhmetshin *et al.* (CMD-2 Collaboration), Phys. Lett. B **509**, 217 (2001).
 - [3] Yu. M. Shatunov *et al.*, in Proceedings of the 7th European Particle Accelerator Conference, Vienna, 2000, p. 439, <http://accelconf.web.cern.ch/AccelConf/e00/PAPERS/MOP4A08.pdf>.
 - [4] M. N. Achasov *et al.*, Nucl. Instrum. Methods Phys. Res., Sect. A **598**, 31 (2009); V. M. Aulchenko *et al.*, *ibid.* **598**, 102 (2009); A. Yu. Barnyakov *et al.*, *ibid.* **598**, 163 (2009); V. M. Aulchenko *et al.*, *ibid.* **598**, 340 (2009).
 - [5] M. N. Achasov *et al.* (SND Collaboration), Phys. Rev. D **88**, 054013 (2013).
 - [6] J. Beringer *et al.* (Particle Data Group) Phys. Rev. D **86**, 010001 (2012).

- [7] M. N. Achasov *et al.* (SND Collaboration), J. Exp. Theor. Phys. **103**, 720 (2006).
- [8] B. Aubert *et al.* (BABAR Collaboration), Phys. Rev. D **76**, 092005 (2007); **77**, 119902(E) (2008).
- [9] E. A. Kuraev and V. S. Fadin, Yad. Fiz. **41**, 733 (1985) [Sov. J. Nucl. Phys. **41**, 466 (1985)].
- [10] G. Bonneau and F. Martin, Nucl. Phys. **B27**, 381 (1971).
- [11] A. B. Clegg and A. Donnachie, Z. Phys. C **62**, 455 (1994).
- [12] F. E. Close, A. Donnachie and Yu. S. Kalashnikova, Phys. Rev. D **65**, 092003 (2002).
- [13] N. N. Achasov and V. A. Karnakov, JETP Lett. **39**, 342 (1984).
- [14] M. N. Achasov *et al.* (SND Collaboration), JETP Lett. **92**, 80 (2010).
- [15] B. Aubert *et al.* (BaBar Collaboration), Phys. Rev. D **73**, 052003 (2006).
- [16] B. Aubert *et al.* (BaBar Collaboration), Phys. Rev. D **77**, 092002 (2008).
- [17] M. N. Achasov *et al.* (SND Collaboration), Nucl. Phys. B **569**, 158 (2000).
- [18] V. P. Druzhinin, arXiv:0710.3455 [hep-ex].